Negative rotatable anisotropy in IrMn/Cr/Co thin films

S. Nicolodi,[1] L. G. Pereira,[1] A. Harres,[1] G. M. Azevedo,[1] J. E. Schmidt,[1] I. García-Aguilar,[2] N. M. Souza-Neto,[2] C. Deranlot,[3] F. Petroff,[3] and J. Geshev[1]

[1]*Instituto de Física, URFGS, Porto Alegre, 91501-970 Rio Grande do Sul, Brazil*

[2]*Laboratório Nacional de Luz Síncrotron (LNLS), Campinas, 13083-970 São Paulo, Brazil*

[3]*Unité Mixte de Physique CNRS/Thales, 91767 Palaiseau and Université Paris-Sud, 91405 Orsay, France*

(Received 18 March 2012; published 29 June 2012)

This work presents modifications of the magnetic properties of polycrystalline IrMn/Cr(t_{Cr})/Co films where the Cr spacer thickness t_{Cr} was varied between 0.25 and 3 nm. High-resolution transmission electron microscopy, x-ray diffractometry and reflectivity, as well as x-ray absorption near-edge structure were used for the structural characterization of the films; static magnetization curves as well as ferromagnetic resonance measurements were employed for the magnetic characterization. Decrease of the exchange-bias field and considerable and nonmonotonous enhancement of the coercivity with t_{Cr} were observed. The films' anisotropy parameters were extracted from the experimental angular variations of the resonance field and from the hard-axis magnetization curves via numerical simulations. It was obtained that the two phenomena studied, namely, the exchange bias and rotatable anisotropy, have different origins. The rotatable anisotropy was ascribed to Cr interface coupled antiferromagnetically with the Co atoms. On the other hand, the occurrence of exchange bias, even for the film with the thickest Cr layer, was attributed to uncompensated spins at the topmost IrMn interface. Together with the significant increase with t_{Cr} of the rotatable anisotropy field, near saturation it is antiparallel to the external magnetic field.

DOI: 10.1103/PhysRevB.85.224438 PACS number(s): 75.70.Cn, 75.30.Gw, 75.60.−d, 75.30.Et

I. INTRODUCTION

The magnetic exchange bias (EB) has been extensively studied both theoretically and experimentally during recent decades.[1–4] One of the contentious topics related to the effect concerns the range of the antiferromagnet/ferromagnet (AF/FM) interactions. While nearest-neighbor coupling is normally reported,[5–9] long-range contributions to EB across a spacer layer (SL) have also been asserted.[10] The coupling strength has been observed to decay exponentially in AF/SL/FM structures with metal SLs.[5,10] In FeMn/SL/FeNi films with very thin SLs (Cu or Cr), Mewes *et al.*[6] have found, in addition to a monotonous decay, an oscillation of the coupling. Such an oscillation has also been observed in NiO/Cu/NiFe films near to the Néel temperature T_N, while the EB field H_{eb} has been found to decrease monotonically with the SL's thickness at low temperature.[11]

Another stimulating question concerns the rotatable anisotropy (RA) that emerges from uncompensated spins (UCS) at the FM/AF interface which accompany the rotation of the FM's magnetization, **M**. In ferromagnetic resonance (FMR) experiments on EB systems, the frequently observed isotropic shift of the resonance field H_{res} has been attributed[12] to unidirectional RA with the corresponding energy term $-\mathbf{M}\cdot\mathbf{H_{RA}}$, with $\mathbf{H_{RA}}$ being the rotatable anisotropy field. When irreversible magnetization processes are involved, e.g., in hysteresis loop traces, uniaxial RA energy of the form $-(\mathbf{M}\cdot\mathbf{H_{RA}})^2$ has been considered.[13] Such an approach explains qualitatively both the H_{res} shift and the increased coercivity in bilayers with polycrystalline AF. Variations of both magnitude and easy-axis direction of the RA as the external magnetic field H is changed[14] or an RA easy magnetization axis tilted from the EB direction[15,16] were also studied.

Studies of EB systems with Co/Cr interfaces are, to date, rather scarce, most probably due to the difficulty of producing Co/Cr samples of good quality given that Co and Cr exhibit different stacking and lattice constants in their respective stable bulk configurations.[17] Moreover, Cr shows complex behavior of an incomensurate spin-density wave in bulk,[18] also expected in Cr substrate systems. Nevertheless, EB with T_N as high as 425 K has been observed in Co/Cr (35 nm) bilayers.[19]

The present work reports experimental results obtained on a series of polycrystalline IrMn/Cr(t_{Cr})/Co films, where the thickness of the chromium layer t_{Cr} is varied. We used numerical simulations in order to extract the anisotropy parameters from the experimental variations of H_{res} and from the hard-axis magnetization curves for **H** applied in the film's plane. We found a substantial and nonmonotonous increase of the coercivity H_C and of the rotatable anisotropy with t_{Cr}. We ascribed the RA to the Cr interface coupled antiferromagnetically with the Co atoms and, most importantly, we obtained that near saturation $\mathbf{H_{RA}}$ and **H** are *antiparallel*. On the other hand, the nonzero bias measured even for the film with the thickest Cr layer was attributed to UCS at the topmost IrMn interface.

II. EXPERIMENTAL

Ru (15 nm)/$Ir_{20}Mn_{80}$ (15 nm)/Cr/Co (5 nm)/Au (10 nm) films for t_{Cr} equal to 0, 0.25, 0.5, 0.75, 1.0, 1.5, 2.0, and 3.0 nm were deposited by magnetron sputtering onto Si(100) substrates (base pressure 5.0×10^{-8} mbar, Ar pressure 2.5×10^{-3} mbar for the deposition of Ru, Cr, Co, and Au, and 1.0×10^{-2} mbar for $Ir_{20}Mn_{80}$ at room temperature (RT) in DC mode.

Conventional x-ray diffractometry (XRD), x-ray reflectometry (XRR), grazing incidence x-ray absorption near edge structure (GI-XANES), transmission electron microscopy (TEM), and high-resolution transmission electron microscopy (HRTEM) were used for the structural characterization.

An alternating gradient-field magnetometer was used for tracing RT in-plane magnetization curves. Overestimation of the EB effect due to minor loop effects[4,20,21] has been avoided by achieving effective saturation of the samples using a sufficiently high maximum magnetic field of 2 kOe. We also employed the FMR technique at the X-band microwave excitation frequency of 9.79 GHz at RT. The samples were mounted on the tip of a goniometer, thus obtaining H_{res} versus the in-plane field angle ϕ_H ($\phi_H = 0^\circ$ for **H** applied along the EB direction); the accuracy was 0.5° for ϕ_H and 0.1 Oe for the absorption field.

After determining the EB direction induced during the magnetron sputtering of the films which showed in-plane anisotropy (as-deposited films with $t_{Cr} \geqslant 1.0$ nm turned to be magnetically isotropic in their planes), each film was subjected to annealing for 15 min upon 2.4 kOe field applied along the EB direction (or at an arbitrary chosen one if $t_{Cr} \geqslant 1.0$ nm) at $210(\pm 2)\,^\circ$C in vacuum with a pressure better than 10^{-6} mbar. This is the method most used for establishing EB; ion bombardment[22,23] in the presence of a magnetic field, application of sufficiently strong magnetic field at temperatures lower than T_N,[24,25] or even the remnant magnetization of the FM acquired prior to cooling may also set the EB.[26]

III. RESULTS AND DISCUSSION

First, a detailed structural characterization of our films was performed. Cross-section TEM and HRTEM, carried out with a JEOL JEM-2100 microscope with LaB_6 electron gun operating at 200-kV accelerating voltage, were performed on all annealed films. Well-defined polycrystalline layers with quite sharp interfaces [with the exception of the IrMn/(Co-Cr) one, see below] are observed, where the estimated thicknesses of the Ru, IrMn, and Au layers practically coincide with the projected ones. Intriguingly, it is virtually impossible from TEM (Fig. 1) and/or HRTEM (Fig. 2) images to discriminate between the Cr and Co individual layers for all samples of the series, and it is worth noting that the total Cr/Co bilayer thicknesses match precisely with the expected ones for all films, as exemplified in these images.

Figure 2 shows HRTEM image of the film with $t_{Cr} = 3$ nm. The lattice fringes given in the insets were obtained by selecting only the (111) reflections in different regions, with circular masks from the corresponding fast Fourier transforms

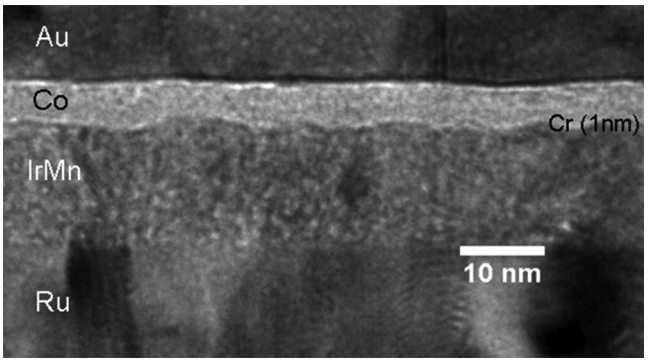

FIG. 1. TEM image of the film with $t_{Cr} = 1.0$ nm.

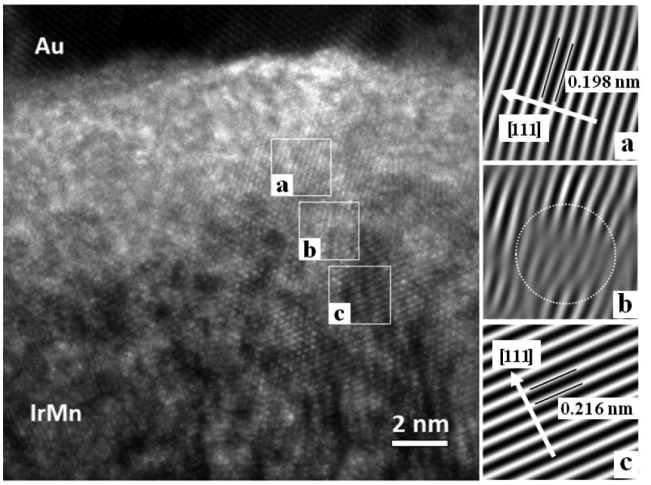

FIG. 2. HRTEM image of the film with $t_{Cr} = 3$ nm. The insets show fast Fourier filtered images obtained from the previous fast Fourier transforms reconstructed with only the (111) reflections on the selected regions. Panels (a) and (c) give the respective interplanar spacing, and the circle in (b) shows a location of misfit dislocations.

to reconstruct filtered images by inverse fast Fourier transform using the GATAN DIGITAL MICROGRAPH software. Panels (a) and (c) in the right show lattice fringes that appear on Co and IrMn regions. The estimated lattice spacings of 0.198 and 0.216 nm correspond to the Co and IrMn fcc {111} planes, respectively. Panel (b) corresponds to the Cr region, and the circle highlights misfit dislocations. The above analysis supports the idea that there is a significant Cr/Co interdiffusion/mixture in all samples. The XRD spectra, obtained at RT employing Cu Kα radiation, showed an fcc structure of the IrMn and Co layers and that these are highly ⟨111⟩ textured. It was not possible to identify the respective bcc Cr(110) peak since it is masked by the Co(111) peak. Simulations of the XRR spectra of the annealed films through the PHILIPS WINGIXA software package showed that the nominal thicknesses of all layers estimated from the fits match very closely with the respective nominal values.

In order to get further and even more precise information on the Cr/Co bilayer structure and/or the depth profile of the chromium layer, GI-XANES measurements were carried out on selected samples. GI-XANES provides atomic and electronic structural information selective to the chemical element and as a function of depth in layered materials[27] and therefore allows the study of magnetic interfaces in the presented samples. While an in-depth description and interpretation of the results will be published in a forthcoming paper, here we present a comparison of XANES spectra collected for the samples with a Cr layer of 0.25, 0.75, 1.0, and 2.0 nm near the Cr K edge with energy of 5989 eV. Energy calibration was done using a reference chromium foil, and angle calibration was performed for every sample based on the reflectivity signal. X-ray fluorescence as a function of grazing incidence angle θ at a fixed energy above the absorption threshold indicated a complete probe of the chromium layer for all samples when $\theta = 2.0^\circ$. XANES for this grazing angle for each sample are shown in Fig. 3. Thicker layers have a bcc chromium structure and differ remarkably from those with

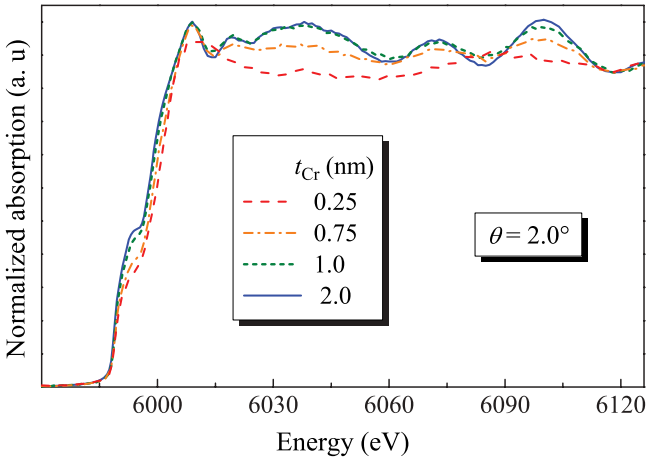

FIG. 3. (Color online) XANES for samples with $t_{Cr} = 0.25$, 0.75, 1.0, and 2.0 nm measured at grazing incidence angle $\theta = 2.0°$ probing the whole Cr layer. The clear difference between the spectra evidences an evolution in the atomic configuration from amorphouslike to a crystalline structure.

$t_{Cr} = 0.25$ and 0.75 nm, where the crystalline structure is lost and more amorphouslike spectra are observed. Since high-angle measurements show a convolution of all layers' contributions, in these thinner samples practically the whole chromium layer is interdiffused into the other layers.

Representative easy and hard-axis magnetization hysteresis loops, i.e., those measured with **H** parallel and perpendicular to the EB direction, respectively, are plotted in Fig. 4 for films with $t_{Cr} \leqslant 2.0$ nm. The loops have a well-defined shape typical for single-phase magnetic systems. The evolution of their H_{eb}^{MAG} (MAG denotes a static magnetization measurement)

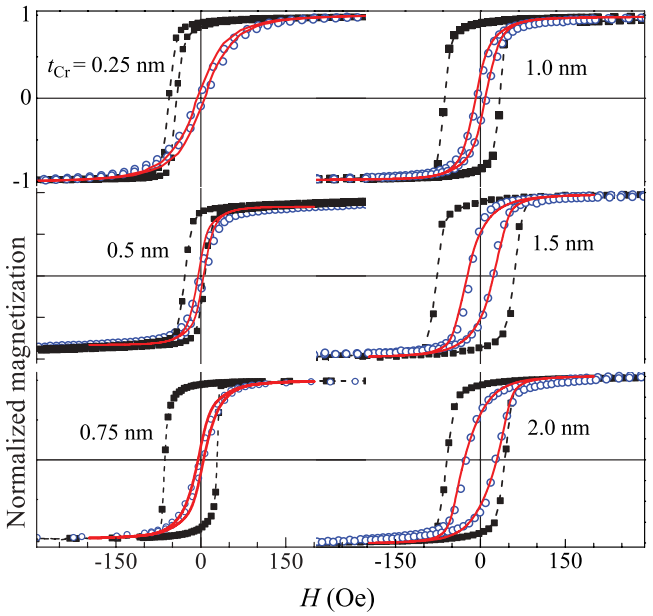

FIG. 4. (Color online) Hysteresis loops traced along the easy (full squares) and hard (empty circles) magnetization directions of films with $t_{Cr} \leqslant 2.0$ nm. The hard-axis fitting curves (solid lines) are simulated using the parameters given in Fig. 6 and the dashed lines are only guides to the eyes.

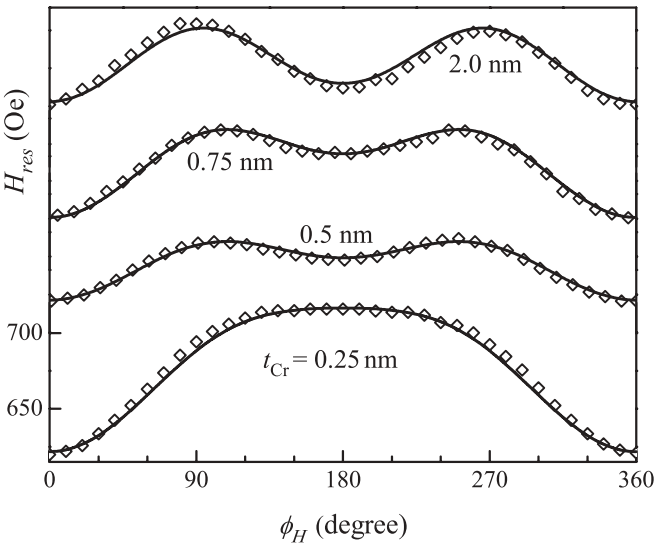

FIG. 5. Angular variations of the resonance field for representative IrMn/Cr/Co samples with $t_{Cr} \leqslant 2.0$ nm. The lines are calculated using the parameters given in Fig. 6. Except for the spectrum for $t_{Cr} = 0.25$ nm, all others are shifted upward vertically for better visualization.

and H_C with t_{Cr}, however, differs significantly from that observed in analogous systems containing nonmagnetic metal or insulator spacers where both field shift and coercivity decrease monotonously with SL thickness and the EB vanishes when the IrMn/Co atomic contact is lost.[8,9,28]

The symbols in Fig. 5 represent the experimentally obtained $H_{res}(\phi_H)$ for the films with $t_{Cr} \leqslant 2.0$ nm, where the lines give the corresponding best-fitting curves calculated through the AF domain-wall-formation model[29,30] with the help of a previously derived expression[31] for $H_{res}(\phi_H)$. The variations of three of the parameters used in the simulations, i.e., the AF/FM exchange-coupling field H_E [$=J/(M_S t)$, J being the AF/FM exchange-coupling constant, M_S the saturation magnetization of the FM and t its thickness], the FM uniaxial anisotropy field H_U, and H_{RA}, are given in the bottom panel of Fig. 6. The other parameters were kept fixed, namely, the interface AF domain-wall anisotropy field $H_W = 510$ Oe, $M_S = 1400$ emu/cm^3, and $\omega/\gamma = 3.497$ kOe, where ω is the angular frequency of precession and γ is the FM layer's gyromagnetic ratio. It is worth noting that the coupling strength estimated for the film without Cr spacer, $J \approx 0.126$ erg/cm^2, is typical for IrMn/Co exchange coupling.[2,8,32]

The top panel of Fig. 6 gives H_C, H_{eb}^{MAG} together with the EB field obtained from the FMR data of the films defined as[12,33] $H_{eb}^{FMR} = \frac{1}{2}|H_{res}(\phi_H = 0) - H_{res}(\phi_H = \pi)|$ versus t_{Cr}. The variation of $\overline{H}_{res}(t_{Cr}) - \overline{H}_{res}(t_{Cr} = 0)$ is also plotted in this panel, where the here-defined $\overline{H}_{res} = \frac{1}{2}[H_{res}(\phi_H = 0) + H_{res}(\phi_H = \pi)]$ could be considered as an effective mean value of H_{res} for each t_{Cr}. H_C shows a rather unusual and nonmonotonous increase, having a pronounced maximum at $t_{Cr} \approx 1.5$ nm. Cr atoms diffused into grain boundaries in the Co layer may enhance the annealing-induced Co grain isolation, also leading to an increase of H_C;[34] this effect, however, seems to be important for higher annealing temperatures than those used here. As it will be argued later,

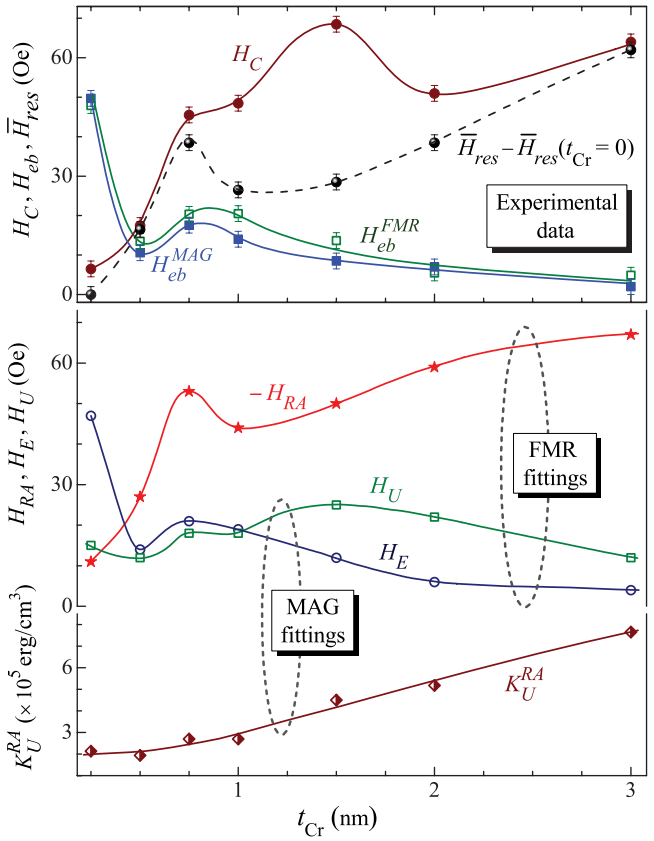

FIG. 6. (Color online) Top: Dependencies of H_{eb}, H_C and $\overline{H}_{res}(t_{Cr}) - \overline{H}_{res}(t_{Cr}) = 0$ on t_{Cr}, where the error bars correspond to the uncertainties in the measuring magnetic fields used in the MAG and FMR experiments. Bottom: Variations of the FMR fitting parameters and those of K_U^{RA}, the latter obtained from the magnetization curve simulations shown in Fig. 4 using H_U and H_E from the FMR fittings and antiparallel exchange coupling ($J' = -0.059$ erg/cm^2) between FM and rotatable grains. Since all H_{RA} values (estimated from the FMR simulations) are negative, $-H_{RA}(t_{Cr})$ is plotted for a better visualization. The lines are guides to the eyes.

the major part of the significant coercivity enhancement of our films should be attributed to the raise of the rotatable anisotropy due to the increase of the Cr content.

Let first discuss the Cr/Co coupling in our IrMn/Cr/Co series. Apart from the local minimum at around $t_{Cr} = 0.5$ nm, both $H_{eb}^{MAG}(t_{Cr})$ and $H_{eb}^{FMR}(t_{Cr})$ present a decrease of the type $H_{eb} \propto \exp(-t_{Cr}/\lambda)$ characteristic for the greater part of the AF/SL/FM systems (see, e.g., Ref. 9 and references therein). However, here the value of the estimated decay length λ of 6 Å for $t_{Cr} \geqslant 0.75$ nm is roughly two times higher than the values normally found in the literature for nearest-neighbor AF/FM coupling, attributed to a direct AF/FM contact through pinholes detected up to SL thickness of $\approx$1 nm. In our films, the shift field decreases rather slowly and persists up to $t_{Cr} =$ 3 nm at least, so the respective coupling does not seem to be of a short-range type.

Due to the AF anisotropy of chromium, the $H_{eb}(t_{Cr})$ variation cannot be explained with the help of the recently proposed intuitive model[35] for the evolution of the EB parameters with the thickness of nonmagnetic SLs. Here we propose that the following mechanisms may act separately or all together and determine the thickness dependence of the EB for the case of a Cr spacer:

(i) When a small amount of Cr is deposited onto IrMn, Cr atoms might diffuse towards the IrMn layer after the annealing. As a result, the IrMn anisotropy will be decreased, thus resulting in the prominent initial decrease of the bias with t_{Cr}.

(ii) With the increase of the effective Cr layer's thickness, the IrMn/Co interface area is gradually reduced at the cost of IrMn/Cr/Co structures. For very small values of t_{Cr}, a portion of the Cr interlayer might still be paramagnetic, given that a certain minimum number of monolayers is required to establish AF order. Its spin alignment is determined by the spin directions in the adjacent IrMn grains. In these configurations, direct exchange between IrMn and Co does not occur and it is mediated by the Cr particles. Part of the Cr grains might have sufficiently strong anisotropy (their magnetizations are, to a certain extent, stabilized by pinning to the IrMn), resulting in EB; the rest of the grains are not magnetically stable enough for EB but will contribute to the RA. Grains of the latter type appear first, as can be inferred from the increase of the RA and H_C in Fig. 6, while H_{eb} only decreases for $t_{Cr} \leqslant 0.5$ nm. Part of the RA grains are transformed into stable ones when t_{Cr} raises to 0.75 nm, and these grains are, most probably, responsible for the observed increase of H_{eb} at $t_{Cr} = 0.75$ nm.

(iii) For further increase of t_{Cr}, Cr grains deposited onto the IrMn ones attain sizes sufficient for a bulklike AF behavior. There is no experimental evidence of exchange coupling between AF grains in metallic polycrystalline AF layers,[36] so the IrMn/Co coupling should cease when their separation by Cr (a weak AF) is accomplished and no bias ought to be detected.

The nonzero H_{eb} of our samples with the thickest Cr layers, however, cannot be due to Cr/Co exchange coupling. Although EB has been observed in Co/Cr at low temperatures, no bias has been detected at RT for t_{Cr} lower than 13 nm.[19] Also, it is well established that, for a constant volume of the FM material, H_{eb} presents a general trend of rise as the AF thickness is increased (starting from usually a few nanometers) and, for thick enough AF layers, it is independent of their thickness. Since our films show the opposite behavior for $t_{Cr} > 1$ nm, one concludes that the (relatively long-range) EB should again be attributed to the UCS at the topmost IrMn interface. It seems that due to the already discussed Cr-Co mixture, even in the films with the thickest Cr layers, there still exist pinholes operating like coupling channels through which the Co layer "senses" some UCS at the top of the IrMn layer.

The competition between the above-described mechanisms probably causes the nonmonotonous $H_{eb}(t_{Cr})$ variation of our series of films.

One of the most important results of the present study is the *negative* RA estimated from the $H_{res}(\phi_H)$ fittings. The variation of $-H_{RA}$ with t_{Cr} is given in Fig. 6, together with those of H_E and H_U. To our knowledge, there are no reports in the literature of negative RA until now. The implication of the negative sign could be better understood with the help of Fig. 7. It shows an experimental $H_{res}(\phi_H)$ and two fitting curves, simulated without RA contribution, which are practically identical to the experimental one, the only difference being that these are shifted (upward or downward) isotropically. The

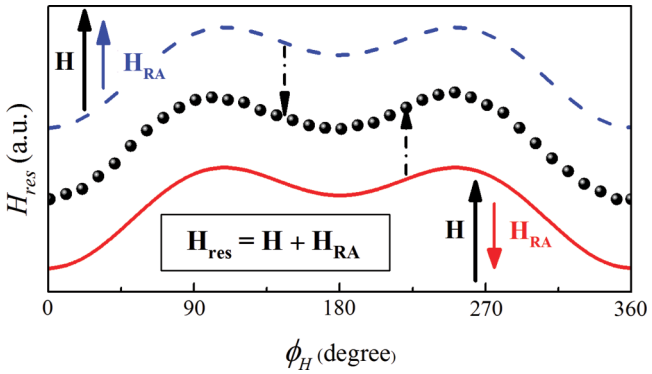

FIG. 7. (Color online) Experimental (symbols) and model $H_{res}(\phi_H)$ curves simulated without taking into account the rotatable anisotropy. The dashed line represents the $\mathbf{H} \parallel \mathbf{H_{RA}}$ case when the fitting curve must be shifted downward. For antiparallel $\mathbf{H}$ and $\mathbf{H_{RA}}$, the shift is upward (solid curve).

inclusion of RA simply reallocates the vertical position of the curves. Positive or negative RA represents a shift toward a lower or upper vertical position corresponding to $\mathbf{H_{RA}}$ roughly parallel or antiparallel to $\mathbf{H}$, respectively.

Recall that an experimentally measured H_{res} is actually the external field necessary for the system to attain resonance. If $\mathbf{H}$ is not the only field acting on the magnetic moments, however, the value of the actual resonance field will be smaller or higher than the H value. In models that take into consideration the RA, $\mathbf{H_{res}} = \mathbf{H} + \mathbf{H_{RA}}$. Therefore, a downward correction corresponds to the usual case of $\mathbf{H_{RA}} \parallel \mathbf{H}$, i.e., the rotatable moments coupled to the FM are practically aligned with $\mathbf{H}$ at resonance. The corrective shift for our samples, on the other hand, is toward an upper position, evidencing that $\mathbf{H_{RA}}$ and $\mathbf{H}$ are *antiparallel*.

Therefore, the magnetic moments responsible for the RA are coupled antiferromagnetically to the FM. In our FMR experiments where the Co layers are nearly saturated, the estimated negative cobalt's RA reflects the fact that the UCSs responsible for the RA and their neighboring Co moments are oppositely directed due to the particular (antiparallel) exchange coupling type. Considering the substantial increase of the RA magnitude with t_{Cr}, one should attribute the RA to the Cr atoms deposited onto (111)-textured IrMn. Izquierdo and Demangeat[17] have performed *ab initio* calculations of the magnetic behavior of Co grown onto Cr substrates with (100), (110), and (111) orientations. They have estimated that for Co/Cr(111), the Cr interface couples antiferromagnetically with the Co atoms and that this type of coupling persists up to more than 30 Cr underlayers (note that Cr bulk is an AF with magnetic moment per atom of about 0.60 μ_B). These authors have also investigated the possible dependence on the Co-Cr distance at the interface considering a small, up to 15%, reduction or expansion of the interface distance, and obtained that the antiferromagnetic coupling is still present and that the Cr atoms have valuable magnetic moments of 1.2 μ_B at the interface for this orientation. Also through *ab initio* calculations, Brovko *et al.*[37] have clearly demonstrated that, on (111) surfaces, Co and Cr in a close-packed dimer are coupled antiferromagnetically.

Thus the antiferromagnetic Cr/Co coupling and valuable Cr magnetic moment explain both the negative RA of our Co films and their coercivity enhancement. The H_{RA} and H_C variations are rather similar, except for 1 nm $\leqslant t_{Cr} \leqslant$ 2 nm. Given that the other magnetic parameters of the system change very little in this Cr thickness interval, the expressed maximum of H_C at $t_{Cr} = 1.5$ nm, not observed in $H_{RA}(t_{Cr})$, should be attributed not to RA but to other sources, e.g., structural changes in the Co layer. It is seen that up to $t_{Cr} = 2$ nm the $\overline{H}_{res}$ and H_{RA} variations are practically identical, indicating that the magnetic properties of the FM layers do not change substantially. The steeper rise of $\overline{H}_{res}$ as compared to H_{RA} for high t_{Cr} might be due to the better separation between the Co and Cr phases, given that the value of H_{res} for $t_{Cr} = 3$ nm is very close to that of an uncoupled Co layer of an analogous system with nonmagnetic insulator SL.[9]

We also performed a series of magnetization loop simulations. However, the particularity of the EB system studied, i.e., H_U several times smaller than $|H_{RA}|$ and the negative sign of the latter estimated from the FMR angular variations, does not allow the prompt use of models that assume constant RA when simulating complete magnetization hysteresis cycles[13] if the anisotropy parameters from the FMR fittings are to be used. We verified that, contrary to what was experimentally observed, such calculations result in anhysteretic curves for all in-plane magnetic field orientations. Thus, we employed a recently developed polycrystalline EB model[38] which considers that, for strong enough interface exchange coupling, the AF layer breaks the adjacent FM into small-sized domains;[39] these domains interact with two types of interfacial grains with UCSs, i.e., stable (or biasing) and rotatable grains. A particular case of this model has proved to be able to account for a rather peculiar EB characteristic, namely, the athermal training effect.[40] Differently from the previous RA models, there are two terms corresponding to effective RA in the energy expression of this model, i.e., that of the magnetic anisotropy of rotatable grains and a term representing the FM/UCS (rotatable) exchange coupling with coupling constant J'. Only hard-axis magnetization curves were considered in view of the fact that the model takes into account coherent grain magnetization reversals.

For the simulation of the model curves plotted in Fig. 4, it was assumed that all grains have uniaxial anisotropy, and while the FM and stable grains (the latter with anisotropy constant of 1.6×10^6 erg/cm^3) have their symmetry axes parallel to the macroscopic EB direction, the easy axes of the RA grains are equally distributed in-plane. A UCS saturation magnetization of 900 emu/cm^3 was assumed as well as a UCS/FM grain volume ratio of 0.1. (For $t_{Cr} = 0.25$ nm only, this ratio was assumed to 0.05.) Antiparallel exchange coupling, i.e., $J' = -0.059$ erg/cm^2, and the same M_S, H_U, and H_E values used in the FMR fittings were also employed. The parameter varied with t_{Cr} in order to fit the experimental hard-axis magnetization loops was the rotatable grains' uniaxial anisotropy constant K_U^{RA}.

The good agreement between simulated and experimental magnetization curves seen in Fig. 4 indicates, once again, the validity of the antiparallel Co/Cr alignment proposition. This is also supported by the variation of K_U^{RA} with t_{Cr} shown in Fig. 6, which follows, in general, that of

$|H_{RA}|$ estimated from the FMR simulations except for $t_{Cr} = 0.75$ nm.

IV. CONCLUSIONS

We have reported experimental and model results obtained on polycrystalline IrMn/Cr/Co films with emphasis on the variations of their exchange-bias parameters with the increase of the Cr layer thickness. The two distinct phenomena studied here, namely, exchange bias and rotatable anisotropy, have different origins. While the rotatable anisotropy was ascribed to the Cr interface coupled antiferromagnetically with the Co atoms, the nonzero exchange bias, observed even for films with rather thick Cr layers, was attributed to uncompensated spins at the topmost IrMn interface. Moreover, we obtained that the rotatable anisotropy field is always antiparallel to the external magnetic field.

ACKNOWLEDGMENTS

We acknowledge LNLS for the synchrotron beam time at the D08B-XAFS2 beamline. The TEM facilities were kindly provided by LCME/UFSC. S.N. thanks M. A. de Sousa and F. Pelegrini for their assistance in the FMR measurements at IF/UFG. This work was supported by the Brazilian agencies CNPq and FAPERGS.

[1] W. H. Meiklejohn and C. P. Bean, Phys. Rev. **102**, 1413 (1956); **105**, 904 (1957).
[2] J. Nogués and I. K. Schuller, J. Magn. Magn. Mater. **192**, 203 (1999).
[3] A. E. Berkowitz and K. Takano, J. Magn. Magn. Mater. **200**, 552 (1999).
[4] J. Nogués, J. Sort, V. Langlais, V. Skumryev, S. Suriñach, J. S. Muñoz, and M. D. Baró, Phys. Rep. **422**, 65 (2005).
[5] L. Thomas, A. J. Kellock, and S. S. P. Parkin, J. Appl. Phys. **87**, 5061 (2000).
[6] T. Mewes, B. F. P. Roos, S. O. Demokritov, and B. Hillebrands, J. Appl. Phys. **87**, 5064 (2000).
[7] M. Gruyters, M. Gierlings, and D. Riegel, Phys. Rev. B **64**, 132401 (2001); J. Wang, J. Appl. Phys. **91**, 7236 (2002); Y. G. Yoo, S. G. Min, and S. C. Yu, J. Magn. Magn. Matter **304**, e718 (2006).
[8] J. Geshev, S. Nicolodi, L. G. Pereira, L. C. C. M. Nagamine, J. E. Schmidt, C. Deranlot, F. Petroff, R. L. Rodríguez-Suárez, and A. Azevedo, Phys. Rev. B **75**, 214402 (2007).
[9] S. Nicolodi, A. Harres, L. G. Pereira, J. E. Schmidt, M. A. de Sousa, F. Pelegrini, A. D. C. Viegas, C. Deranlot, F. Petroff, and J. Geshev, J. Appl. Phys. **110**, 063922 (2011).
[10] N. J. Gökemeijer, T. Ambrose, and C. L. Chien, Phys. Rev. Lett. **79**, 4270 (1997).
[11] M.-T. Lin, C. H. Ho, C.-R. Chang, and Y. D. Yao, Phys. Rev. B **63**, 100404 (2001).
[12] R. D. McMichael, M. D. Stiles, P. J. Chen, and W. F. Egelhoff Jr., Phys. Rev. B **58**, 8605 (1998).
[13] J. Geshev, L. G. Pereira, and J. E. Schmidt, Phys. Rev. B **66**, 134432 (2002).
[14] J. K. Kim, S. W. Kim, K. A. Lee, B. K. Kim, J. H. Kim, S. S. Lee, and D. G. Hwanga, C. G. Kim, and C. O. Kim, J. Appl. Phys. **93**, 7714 (2003).
[15] F. Radu, A. Westphalen, K. Theis-Bröhl, and H. Zabel, J. Phys.: Condens. Matter **18**, L29 (2006).
[16] J. McCord, C. Hamann, R. Schäfer, L. Schultz, and R. Mattheis, Phys. Rev. B **78**, 094419 (2008).
[17] J. Izquierdo and C. Demangeat, Phys. Rev. B **62**, 12287 (2000).
[18] E. Fawcett, Rev. Mod. Phys. **60**, 209 (1988).
[19] F. Y. Yang and C. L. Chien, J. Appl. Phys. **93**, 6829 (2003).
[20] L. Klein, Appl. Phys. Lett. **89**, 036101 (2006).
[21] J. Geshev, J. Magn. Magn. Mater. **320**, 600 (2008).
[22] J. Fassbender, D. Ravelosona, and Y. Samson, J. Phys. D: Appl. Phys. **37**, R179 (2004); J. Fassbender and J. McCord, J. Magn. Magn. Mater. **320**, 579 (2008).
[23] D. Schafer, J. Geshev, S. Nicolodi, L. G. Pereira, J. E. Schmidt, and P. L. Grande, Appl. Phys. Lett. **93**, 042501 (2008); D. Schafer, P. L. Grande, L. G. Pereira, and J. Geshev, J. Appl. Phys. **109**, 023905 (2011).
[24] J. Nogués, L. Morellon, C. Leighton, M. R. Ibarra, and I. K. Schuller, Phys. Rev. B **61**, R6455 (2000).
[25] J. Nogués, J. Sort, S. Suriñach S, J. S. Muñoz, M. D. Baró, J. F. Bobo, U. Lüders, E. Haanappel, M. R. Fitzsimmons, A. Hoffmann, and J. W. Cai, Appl. Phys. Lett. **82**, 3044 (2003).
[26] N. J. Gökemeijer and C. L. Chien, J. Appl. Phys. **85**, 5516 (1999); A. Paul, C. M. Schneider, and J. Stahn, Phys. Rev. B **76**, 184424 (2007); J. Geshev, L. G. Pereira, and V. Skumryev, Phys. Rev. Lett. **100**, 039701 (2008).
[27] N. M. Souza-Neto, A. Y. Ramos, H. C. N. Tolentino, A. Martins, and A. D. Santos, J. Appl. Cryst. **42**, 1158 (2009).
[28] S. Nicolodi, L. C. C. M. Nagamine, A. D. C. Viegas, J. E. Schmidt, L. G. Pereira, C. Deranlot, F. Petroff, and J. Geshev, J. Magn. Magn. Matter **316**, e97 (2007).
[29] D. Mauri, H. C. Siegmann, P. S. Bagus, and E. Kay, J. Appl. Phys. **62**, 3047 (1987).
[30] J. Geshev, Phys. Rev. B **62**, 5627 (2000).
[31] J. Geshev, L. G. Pereira, and J. E. Schmidt, Phys. Rev. B **64**, 184411 (2001).
[32] A. Harres, S. Nicolodi, L. G. Pereira, J. E. Schmidt, A. D. C. Viegas, and J. Geshev, J. Magn. Magn. Mater. **323**, 2398 (2011).
[33] W. Stoecklein, S. S. P. Parkin, and J. C. Scott, Phys. Rev. B **38**, 6847 (1988).
[34] Y. C. Feng, D. E. Laughlin, and D. N. Lambeth, IEEE Trans. Magn. **30**, 3948 (1994).
[35] J. Geshev, T. Dias, S. Nicolodi, R. Cichelero, A. Harres, J. J. S. Acuña, L. G. Pereira, J. E. Schmidt, C. Deranlot, and F. Petroff, J. Phys. D: Appl. Phys. **44**, 095002 (2011).
[36] K. O'Grady, L. E. Fernandez-Outon, and G. Vallejo-Fernandez, J. Magn. Magn. Mater. **322**, 883 (2010).
[37] O. O. Brovko, P. A. Ignatiev, V. S. Stepanyuk, and P. Bruno, Phys. Rev. Lett. **101**, 036809 (2008).
[38] A. Harres and J. Geshev (unpublished).
[39] Z. Li and S. Zhang, Phys. Rev. B **61**, R14897 (2000).
[40] A. Harres A. and J. Geshev, J. Phys.: Condens. Matter **23**, 216003 (2011).